Application of High Voltage Ratio and Low Ripple Interleaved DC-DC Converter for a Fuel Cell

LONG-YI CHANG, KUEI-HSIANG CHAO and TSANG-CHIH CHANG
Department of Electrical Engineering, National Chin-Yi University of Technology
No.57, Sec. 2, Zhong-Shan Road, Taiping District, Taichung
TAIWAN, R.O.C.
chaokh@ncut.edu.tw

Abstract: - This paper proposes a high voltage ratio and low ripple interleaved boost DC-DC converter, which can be used to reduce the output voltage ripple. This converter transfers the low DC voltage of fuel cell to high DC voltage in DC link. The structure of the converter is parallel with two voltage-doublers boost converters by interleaving their output voltages to reduce the voltage ripple ratio. Besides, it can lower the current stress for the switches and inductors in the system. Finally, some experimental results are made to verify the feasibility of the proposed converter.

Key-Words: Fuel Cell, High Voltage Ratio DC-DC Converter, Low Ripple, Interleaved Converter.

1 Introduction

Owing to worldwide energy crisis and awareness of environmental protection in recent years, to seek for substitute energy has become an important issue. Among many substitute energies, solar energy, wind energy, hydroelectric power, biomass energy and fuel cells are green energies with potential development. As for fuel cells, there tend to have been more and more researches and applications recently. The fuel cell is a clean energy without pollution. Its energy, derived from reversed reaction of electrolyzed water, produces dynamic power. Only water is produced after the reaction; hence, there is hardly any environmental pollution. Fuel cells as a source of power are usually applied to electric hybrid automobiles, distributed electric generation system, portable and stationary power. Among them proton exchange membrane fuel cells are the most commonly used because of the following merits: (1) lower temperature during operation, accordingly leading to rapid turning on and off and rapid reaction to the load change (2) lower operation pressure, thus with higher safety (3) easily set in mode system (4) lower Emission Ratio and higher conversion ratio[1-4].

Although the proton exchange membrane fuel cell has the advantages mentioned above, due to its own activation loss, ohmic loss and concentration loss, the output voltage is lowered as a result of load increase. Namely the fuel cell lowers the output voltage but raises the output current gradually as the output power rises under added load. Thus it is a low voltage high current output equipment. If we can transfer the low voltage produced by the fuel cell to high voltage, sending it to DC Link, there will be a wider range of application[5-13]. In order to upgrade the fuel cell voltage output to the necessary electricity level and avoid the unsteady voltage caused by load change, it's necessary to adjust the fuel cell energy by means of power electronic technique, thus keeping steady the output voltage.

Based on this, presented in this paper is a high voltage ratio interleaved DC-DC converter parallelly connected and further interleaved by means of two sets of voltage-doubler boost converters. So besides the advantages of high voltage ratio converter, also because of the effect of parallel connection, the current is dispersed into four routes, thus lowering the current stress of the switch and inductance. In this way it can withstand the high current output while there is high load. Through the parallel connection of two sets of converters and controlling their interleaved voltage, it is possible to lower the output voltage ripple ratio. Fig. 1 is the structure of the high voltage interleaved DC-DC converter presented in this paper. The fuel cell provides electricity for the dual interleaved voltage-doubler of high voltage ratio converter. Electronic load is used to test the amount of load (light or heavy load);also microcontroller PIC 18F8720 manufactured by Microchip company is used for closed loop control.

2 Fuel Cell

There are a great variety of fuel cells; also there are different ways to classify them. The common approach is to classify them according to the various qualities of the electrolyte. Thus they can be divided into the following six kinds:

1. Proton Exchange Membrane Fuel Cell, PEMFC.
2. Alkaline Fuel Cell, AFC.

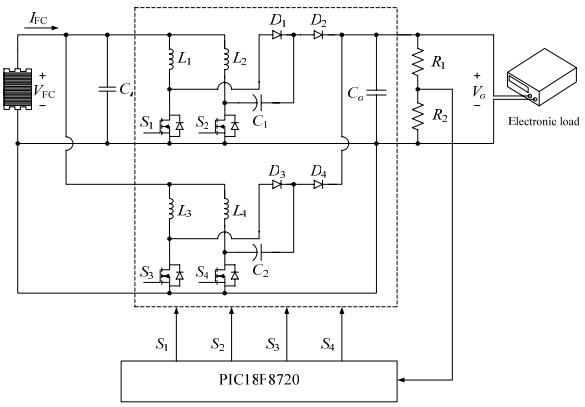

Fig. 1 The system of the presented dual interleaved voltage-doubler of high voltage ratio converter

3. Phosphoric Acid Fuel Cell, PAFC.
4. Molten Carbonate Fuel Cell, MCFC.
5. Solid Oxide Fuel Cell, SOFC.
6. Direct Methanol Fuel Cell, DMFC.

Among them, the proton exchange membrane fuel cell is the best choice when we choose fuel cells for the source of the applied power because of the following reasons: (1) lower operation temperature, thus it can be rapidly turned on and off; (2) lower operation pressure, hence greater safety; (3) it can be easily set into mode system; (4) lower emission ratio and higher conversion ratio.

2.1 Mold-building of Fuel Cells

As for fuel cells, this paper adopts the NEXA^{TM} proton exchange membrane fuel cell produced by Ballard Co. The specifications of this proton exchange fuel cell in shown in Table 1 [14].

In building up the proton exchange membrane fuel cell math model, currently there are many simple precise model parameters and calculation formulae being presented and developed[15, 16]. In this paper we refer to the electrochemistry formulae already presented to build up the math model of the proton exchange membrane fuel cell, also within the range of the load current operation simulate the characteristic curve of the output voltage and power rate of the fuel cell [15, 16].

The math model of the proton exchange membrane fuel cell is shown in (1) and (2)

$$V_{stack} = NV_{FC} \tag{1}$$

$$V_{FC} = E_{Nernst} - V_{act} - V_{ohmic} - V_{con} \tag{2}$$

Therein,

V_{stack}：Stack output voltage.

N：Number of cells forming the stack.

V_{FC}：The output voltage of the fuel cell.

Table 1 Specifications of the Ballard NEXA^{TM} proton exchange membrane fuel cell [14]

Power	Rated Power	1200W
	Operating voltage range	22 to 50V_{DC}
	Voltage at Rated Power	26V
	Current at Rated Power	46A
	Start-up Time	2 minutes
Emissions	Noise	72 dBA
	Water	870 mL/hr
Physical	Dimensions	56 x 25 x 33cm
	Mass	13 kg
Fuel	Purity	99.99 % H_2 (vol)
	Pressure	0.7 to 17.2 bar
	Consumption	<18.5 SLPM

E_{Nernst}：Output voltage produced by every piece of fuel cell in thermodynamics.

V_{act}：Activation loss.

V_{ohmic}：Ohmic loss.

V_{con}：Concentration loss.

And the thermodynamic output voltage of every piece of fuel cell can be shown as follows.

$$E_{Nernst} = 1.229 - 0.85\times10^{-3}(T - 298.15) + 4.31\times10^{-5}T\left[\ln(P_{H2}) + \frac{1}{2}\ln(P_{O2})\right] \tag{3}$$

Therein,

T：Cell temperature (in Kelvin).

P_{H2}：Partial pressures of hydrogen.

P_{O2}：Partial pressures of oxygen.

As for activation loss voltage, it can be shown this way:

$$V_{act} = -[\xi_1 + \xi_2\times T + \xi_3\times T\times\ln(C_{O2}) + \xi_4\times T\times\ln(I_{FC})] \tag{4}$$

Therein,

ξ_1、ξ_2、ξ_3、ξ_4：The parametric coefficient for each cell model.

C_{O2}：The concentration degree of oxygen in the catalytic interface of the cathode.

I_{FC}：Fuel cell current.

And the respective coefficients of the activation loss are:

$$\xi_2 = 0.00286 + 0.0002\times\ln(A) + 4.3\times10^{-5}\times\ln(C_{H2}) \tag{5}$$

$$C_{O2} = P_{O2}/[5.08\times10^{6}\times e^{(-498/T)}] \tag{6}$$

Therein,

A：Cell active area.

C_{H2}：Liquid phase concentration of hydrogen.

As for ohmic loss voltage, it can be shown as follows:

$$V_{ohmic} = I_{FC} \times (R_M + R_C) \tag{7}$$

Therein,

R_M：Resistance coefficient of the membrane.

R_C：Resistance coefficient constant to protons transfer through the membrane.

The resistance coefficient of the membrane therein is:

$$R_M = \rho_M \times L / A \tag{8}$$

Therein,

ρ_M：Specific resistivity of the membrane to the electron flow.

L：Thickness of the membrane.

The resistance coefficient of the membrane can be shown to be:

$$\rho_M = \{181.6 \times [1 + 0.03 \times (I_{FC} / A) + 0.062 \times (T/303)^2 \times (I_{FC} / A)^{2.5}]\} / \{[\lambda - 0.634 - 3 \times (I_{FC} / A) \times e^{[4.18 \times (T-303)/T]}]\} \tag{9}$$

Therein,

λ：Adjustment parameter, the range of which is between 14 and 23.

Concentration loss formula is shown to be:

$$V_{con} = -B \times \ln(1 - j / j_{\max}) \tag{10}$$

Therein,

B：Constant variable depending on the cell type and its working status.

j：Current density of the cell.

j_{max}：Maximum current density.

Therein the current density of the cell is:

$$j = I_{FC} / A \tag{11}$$

Therefore the equivalent circuit of the fuel cell can be worked up as in Fig. 2.

If we take the dynamic response of the fuel cell into consideration, when two different substances come into contact, or the load current flows from one end to the other, accumulation of charge is produced on the contact area. In the fuel cell, the layer of change between the electrode and electrolyte (or compact contact face) will accumulate electric charge and energy, whose action is similar to capacitance. So when the load current changes, these will be charge and discharge phenomena happening on the charge layer. Meanwhile activation loss voltage and concentration loss voltage will be under the influence of transient response, causing delay. But ohmic loss voltage will not be influenced or delayed. We can take this into consideration to let first order lag exist in activation loss voltage and concentration loss voltage. Thus its dynamic response equation can be shown to be[15, 16]:

$$V_{FC} = E_{Nernst} - V_{ohmic} - V_c \tag{12}$$

$$\frac{dV_c}{dt} = \frac{I_{FC}}{C} - \frac{V_c}{\tau} \tag{13}$$

$$\tau = C \times R_a \tag{14}$$

Therein,

τ：Time constant.

C：The equivalent capacitance of the system.

V_c：Dynamic voltage of the fuel cell.

R_a：Equivalent resistance.

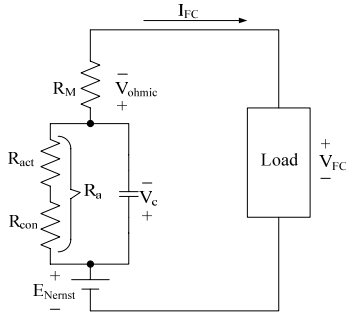

Fig. 2 The equivalent circuit of the fuel cell

The analysis shown above can be used to build up the mathematic model of the proton exchange membrane fuel cell so as to carry on the simulation analysis of the system.

2.2 The Simulation of the Fuel Cell

In this paper PSIM simulation software is used to build up the simulated model of the proton exchange membrane fuel cell. Its composition module is shown in Fig. 3, in which the upper right increased k value is 42, representing the stack amount of the single cell in the cell stack. The simulated circuit of the equivalent capacitance dynamic action is shown in Fig. 4.

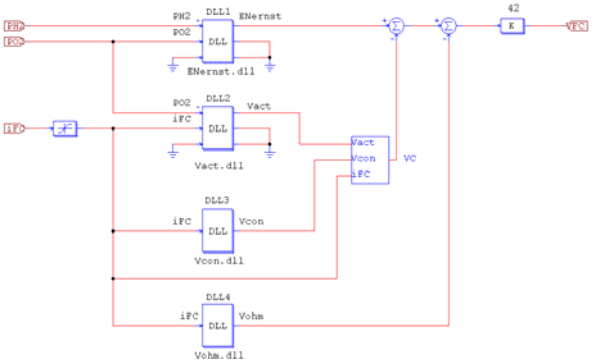

Fig. 3 The fuel cell model built up by means of PSIM software

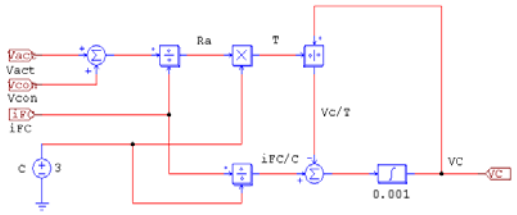

Fig. 4 The simulated circuit of capacitance equivalent dynamic action built up by means of PSIM software

The DLL in Fig. 3 is the dynamic link library of PSIM simulation software. Through software Microsoft Visual C++ 6.0, the necessary DLL file for linking can be set up. By means of Microsoft Visual C++ 6.0, we can make use of programs to write the mathematic formulae in them, saving the trouble of building up numerous inner circuit figures.

After building up fuel cell module, we have its load current operated within fixed rate and value. The hydrogen and oxygen pressures are respectively set up at 1 bar. The characteristic curve of the simulated fuel cell output voltage and power rate is shown in Fig. 5. The upper part of Fig. 5 is the curve of the current and voltage of the fuel cell, while the lower part is the power rate curve. Compared with Fig. 7, the actual measuring output curve of Ballard Co. NEXA^{TM} fuel cell, we can find both of the curves of the output characteristics are closely similar. Only because the curve of Fig. 6 is formed by connecting from point to point, it follows that there is slight difference between them.

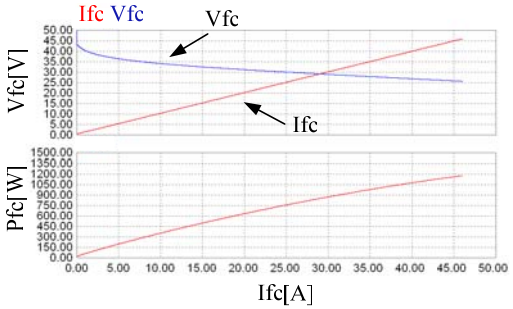

Fig. 5 The curve of the fuel cell output by means of PSIM software simulation

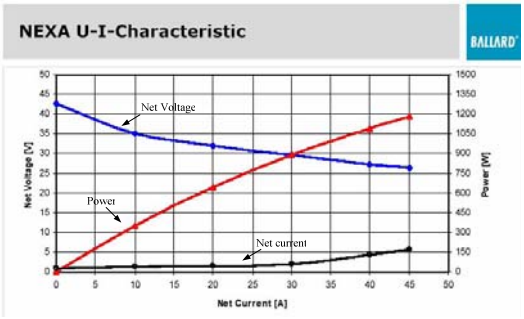

Fig. 6 The curve of the actual measuring output of Ballard Co. NEXA^{TM} fuel cell [14]

3 Single Set of Voltage-Doubler Boost Converter

Shown in Fig. 7 is the circuit structure of single set voltage-doubler boost converter[17, 18]. It is made up of interleaved boost converters with a clamp capacitor C_1. The circuit structure is simple and it can reach the same high voltage ratio with lower duty cycle. Therefore, it can reduce the conduction loss of the switch, to further upgrade the efficiency of the whole converter. The work theorem of the whole circuit can be divided into four operation modes, of which the equivalent circuits are respectively shown in Fig. 8(a)-(d).

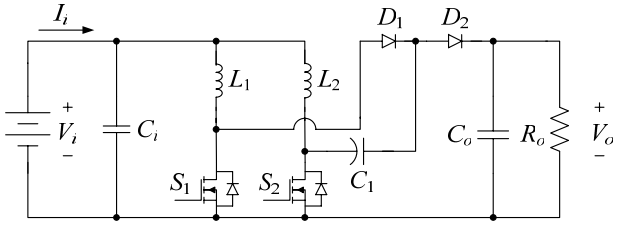

Fig. 7 Circuit structure of voltage-doubler boost converter

The equivalent circuits of mode 1 and mode 3 are exhibited in Fig. 8(a) and (c). In this situation, switches S_1 and S_2 are turned on. Input voltage V_i stays between inductance L_1 and L_2, making the inductance current increase linearly and begins to deposit energy, and the load current is provided by capacitor C_o. The change of the inductance current i_{L1} and i_{L2} can be shown in (15)

$$V_i = L_1 \frac{di_{L1}}{dt} = L_2 \frac{di_{L2}}{dt} \tag{15}$$

Fig. 8(b) is the equivalent circuit in mode 2, in which switch S_1 is turned off while S_2 is turned on. The inductance current in forward direction conducts diode D_1. In the meantime inductance L_1 voltage releases energy to clamp capacitor C_1, charging capacitor C_1 while inductance L_2 goes on depositing energy. The change of the inductance current i_{L1} can be shown in (16).

$$\frac{di_{L1}}{dt} = \frac{V_i - V_{C1}}{L_1} \tag{16}$$

The equivalent circuit of mode 4 is exhibited in Fig. 8(d), in which switch S_1 is turned on and switch S_2 is turned off. The inductance current in forward direction conducts Diode D_2. Then inductance L_2 and clamp capacitor C_1 simultaneously release energy to output capacitor C_o and load. The change of inductance current i_{L2} can be shown in (17).

$$\frac{di_{L2}}{dt} = \frac{V_i + V_{C1} - V_O}{L_2} \tag{17}$$

Through the analysis of the four modes mentioned

above, only V_{C1} capacitor voltage is an unknown variable. According to circuit structure and KVL theorem, inductance L_1, L_2 and the voltage of diode D_1 plus clamp capacitor voltage V_{C1} should be zero, and in steady state the average voltage of inductance L_1 and L_2 is zero. Therefore it is known that the average voltage of D_1 is identical with clamp capacitor voltage V_{C1}. The waveform of D_1 voltage is exhibited in Fig. 9, so the clamp capacitor voltage V_{C1} can be shown in (18).

$$V_{C1} = V_{D1,avg} = \frac{V_O}{2} \tag{18}$$

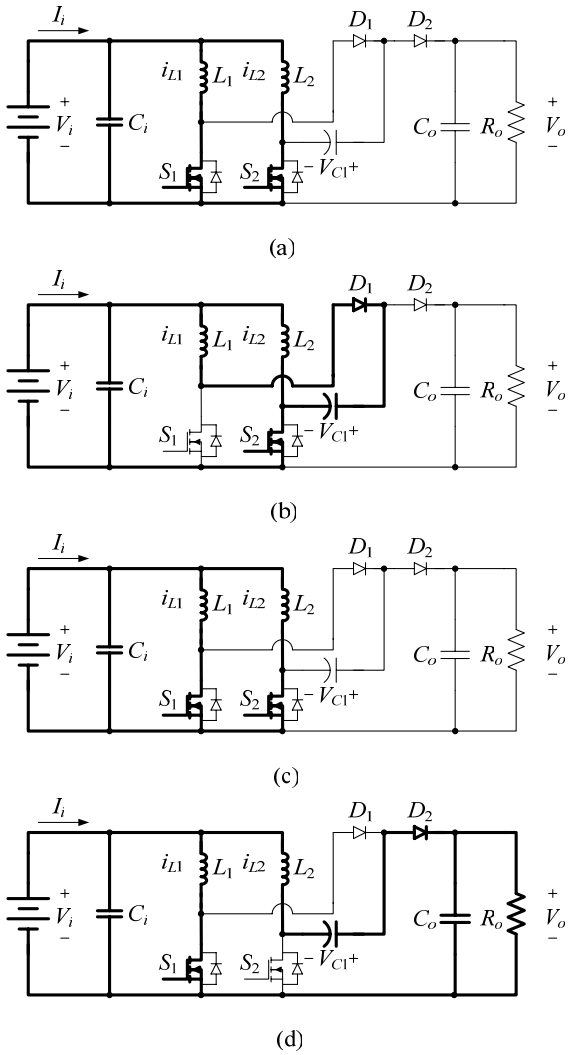

Fig. 8 The four switch modes of voltage doubler boost converter in the duty cycle：(a) model 1 (b) model 2 (c) model 3 (d) model 4

After getting the clamp capacitor voltage, we work out (15) (17) according to volt-second balance theorem and get (19). Then carry in (18) to work out (20). Therefore we can infer that the voltage increase of the converter is shown in (21), in which T is the switching cycle, D is the duty cycle and f is the switching frequency.

$$\frac{V_i - V_{C1}}{L_1} \times (1-D)T + \frac{V_i}{L_1} DT = 0 \tag{19}$$

$$\frac{V_i - (V_O/2)}{L_1} \times (1-D)T + \frac{V_i}{L_1} DT = 0 \tag{20}$$

$$V_O = \frac{2V_i}{1-D} \tag{21}$$

From (21) it is known that voltage-doubler boost converter can reach the same high voltage ratio with shorter duty cycle. Moreover on account of the added clamp capacitor, the voltage of the switch can be reduced to only half of the output voltage. This can be known from the switch voltage of (22) and (23) while operating under mode 2 and mode 4.

$$V_{ds1,\max} = V_{C1} = \frac{V_O}{2} \tag{22}$$

$$V_{ds2,\max} = V_{C1} = \frac{V_O}{2} \tag{23}$$

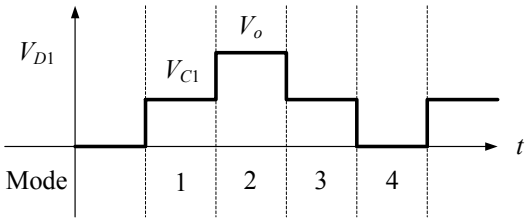

Fig. 9 Voltage waveform of diode D_1 under each mode

The output and input power can be shown respectively in (24) and (25).

$$P_O = \frac{V_O^{\,2}}{R} \tag{24}$$

$$P_i = V_i I_i = V_i \times (I_{L1} + I_{L2}) \tag{25}$$

From (25), assuming L=L_1=L_2, it follows:

$$P_i = V_i I_i = V_i \times 2I_L \tag{26}$$

If there is no power loss of the converter, then P_o=P_i with the following result.

$$V_i \times 2I_L = \frac{V_O^{\,2}}{R} = \frac{(\frac{2V_i}{1-D})^2}{R} = \frac{4V_i^2}{(1-D)^2 R} \tag{27}$$

$$I_L = \frac{2V_i}{(1-D)^2 R} \quad ; \; I_L \in \{I_{L1}, I_{L2}\} \tag{28}$$

The waveform of inductance current is exhibited in Fig. 10, in which though i_{L1} and i_{L2} waveforms are in complementary relation, its maximum and minimum inductance current are the same. Hence based on I_{L1}, the related formulae of the maximum and minimum inductance current are respectively shown in (29) and (30).

$$I_{L1,\max} = I_{L1} + \frac{\Delta i_{L1}}{2} = \frac{2V_i}{(1-D)^2 R} + \frac{V_i DT}{2L_1} \tag{29}$$

$$I_{L1,\min} = I_{L1} - \frac{\Delta i_{L1}}{2} = \frac{2V_i}{(1-D)^2 R} - \frac{V_i DT}{2L_1} \quad (30)$$

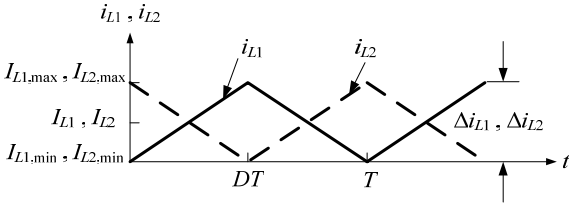

Fig. 10 The waveform of the change of inductance current

The condition on which the converter can be operated in continuous current mode is that $i_{L1,\min}$ and $i_{L2,\min}$ should at least be greater than zero. So the boundary condition of continuous and discontinuous inductance current is:

$$I_{L1,\min} = 0 = \frac{2V_i}{(1-D)^2 R} - \frac{V_i DT}{2L_1} \quad (31)$$

So we get

$$L_{1,\min} = \frac{D(1-D)^2 R}{4f} \quad (32)$$

Because the maximum and the minimum induction current of inductance L_1 and L_2 are the same, the minimum induction rates derived from L_1 and L_2 are identical. Hence if the converter is to be operated in the continuous current mode, inductance L_1 and L_2 must at least be greater than or equal to $L_{1,\min}$.

From the mathematic function $D(1\text{-}D)^2$ of (32), it can be observed if D value is at 1/3, the mathematic function $D(1\text{-}D)^2$ will have the greatest value, which also means the greatest D value created by (32) is 1/3. Hence in designing inductance, when D as 1/3 is substituted into (32), and let the inductance value derived from calculation be multiplied by surplus value 1.25, it can be assured that the inductance current can really work in the continuous current mode.

The so-called light load and heavy load in this paper, their load impedances are respectively 2,020 Ω and 450 Ω. So at switching frequency 15 kHz, heavy load duty cycle about 0.85 when it is substituted into (32), the result is that in order to let the current continue under light load, the least inductance should be 6.23 mH, while under heavy load it should be 179 μH. In this paper 260 μH is the option to make it possible to be in continuous current conduction mode under heavy load.

The change of output capacitor current is shown in the i_{Co} of Fig. 11. From Fig. 11 we know the amount of capacitor electric charge change as

$$|\Delta Q| = \frac{V_O DT}{R_O} = C_O \Delta V_O \quad (33)$$

Then its voltage ripple ratio may be expressed as follows.

$$\frac{\Delta V_O}{V_O} = \frac{DT}{R_O C_O} \quad (34)$$

So the result is

$$C_O = \frac{D}{R_O f(\Delta V_O / V_O)} \quad (35)$$

Therefore in the converter, we can decide the size of the capacitor according to the amount of voltage ripple ratio. From (35) it is observed that the output capacity and duty cycle are in linear relation. It means the designed output capacity must be greater than the required capacity with the greatest duty cycle. In this paper voltage ripple ratio is set at 5%. When it is substituted into (35), the output capacity is 2.5 μF. So 150 μF is selected to make the voltage ripple ratio lower than 5%.

By means of the above-described working mode of the converter, the switch control signal in the circuit, inductance and capacity current waveform can be exhibited in Fig. 11, and its input voltage ripple and current ripple can be shown in (36) and (37)

$$\begin{aligned} \Delta I_i &= \left(\frac{V_O/2 - V_i}{L_n} - \frac{V_i}{L_n}\right)(1-D)T \\ &= \frac{V_O - 4V_i}{2L_n}(1-D)T \;;\; L_n \in \{L_1,\ L_2\} \end{aligned} \quad (36)$$

$$\Delta V_{Co} = I_O DT \quad (37)$$

From (36) it is known that voltage-doubler boost converter has the advantage of lower input current but the amount of its output voltage ripple is the same as the traditional high voltage converter. Hence in this paper we set forth an ameliorated interleaved voltage-doubler boost converter. By means of the original voltage-doubler boost converter parallelly connected, making output voltage interleaved, so as to reduce output voltage ripple, the flaw of greater output voltage is further ameliorated.

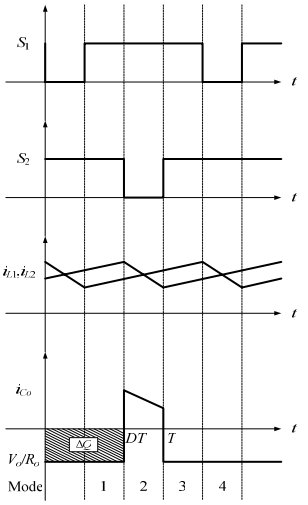

Fig. 11 The switch signal, inductance and capacity waveform under each operation mode

4 The Presented Dual Interleaved Voltage-Doubler of High Voltage Ratio Converter

The circuit structure of the dual interleaved voltage-doubler of high voltage ratio converter presented in this paper is shown in Fig. 12. By means of parallelly connected original voltage-doubler boost converter to have the two sets of upper and lower voltage mutually interleaved, we can lower its output voltage ripple by controlling one set of their switch control signals to make its output voltage ripple offset that of the other set. In controlling both the upper and the lower sets of switches S_1、S_2 and S_3、S_4 to make S_1、S_2 and S_3、S_4 switch control phase discrepancy 180^o lead to voltage ripple phase displacement, the function of lowering voltage ripple is thus achieved. And because the interleaved switches of these two sets of voltage-doubler boost converters make the input current circuit divide into four routes, thus further lowering the current stress of the inductance and switch, it is possible to withstand the high current of the output of the fuel cell under heavy load. Also it is controlled by microcontroller PIC18F8720. In this way the output voltage can be kept steady at a fixed value.

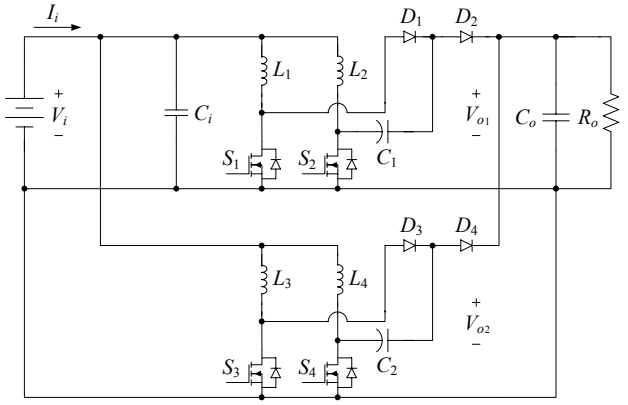

Fig. 12 The circuit structure of dual interleaved voltage-doubler of high voltage ratio converter

Fig. 13 shows the control signal, inductance current, and output voltage ripple waveforms in the circuit. From Fig. 13 are observed the output voltage ripples of the two converters V_{O1} and V_{O2}. Through the phase displacement of the switch control signal, the phase displacement of two sets of voltage ripples is brought about, thus resulting in the effect of lowering the output voltage ripple.

5 Experimental Results

In order to prove the feasibility of the dual interleaved voltage-doubler of high voltage ratio converter set forth in this paper, a test will be carried on under two different loads. The fuel cell produces output voltage about 26 to 43 V, to be upgraded to 300 V, and the electronic load is respectively adjusted at 2,020 Ω (about output power 43 W) and 450 Ω (about output power 200W) under test.

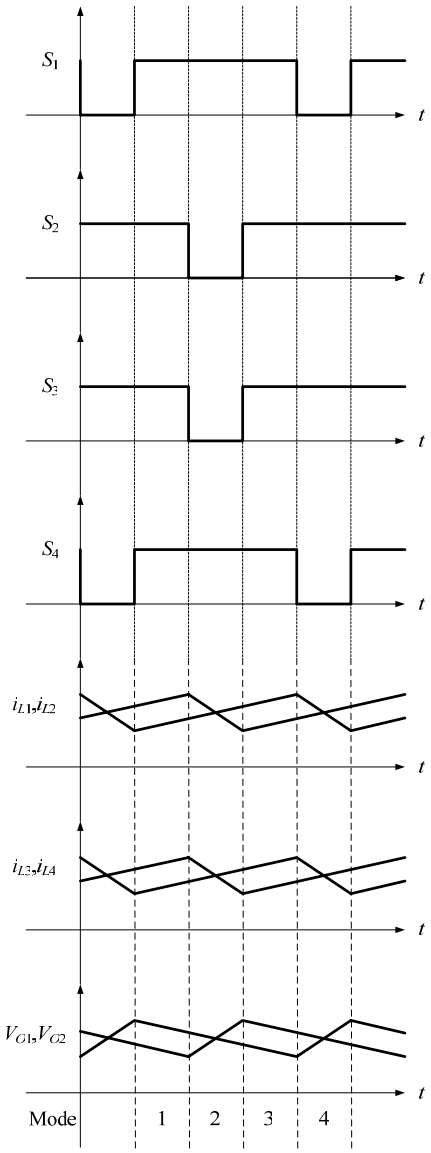

Fig. 13 The ripple waveforms of switch control signal inductance current and output voltage under each operation mode

Fig. 14 is the waveforms of the switch signal control in dual interleaved voltage-doubler of high voltage ratio converter. Switches S_1、S_3 and S_2、S_4 have respective control phase discrepancy 180^o. Figs. 15 and 16 show the waveforms of switch signal and the waveforms of fuel cell output voltage and switch output voltage respectively under output power 43 W and 200 W. From the figures it is observed that under different loads, by controlling the duty cycle of the switch signal, the output voltage can be kept steady at 300 V.

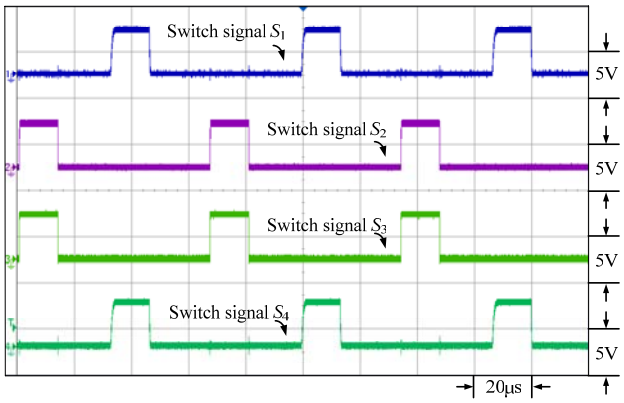

Fig. 14 The switch signal waveforms of dual interleaved voltage-doubler of high voltage ratio converter

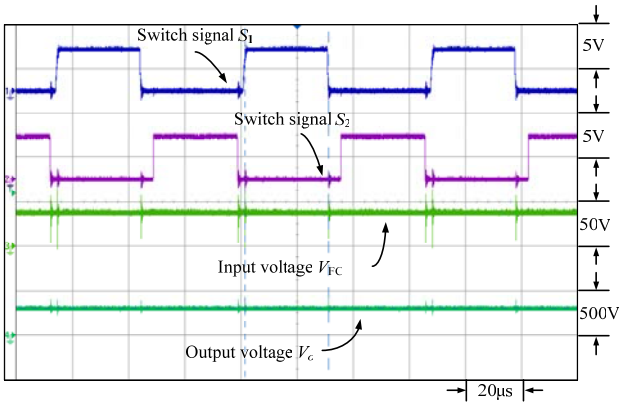

Fig. 15 The switch signal and input/output voltage waveforms under output power 43 W

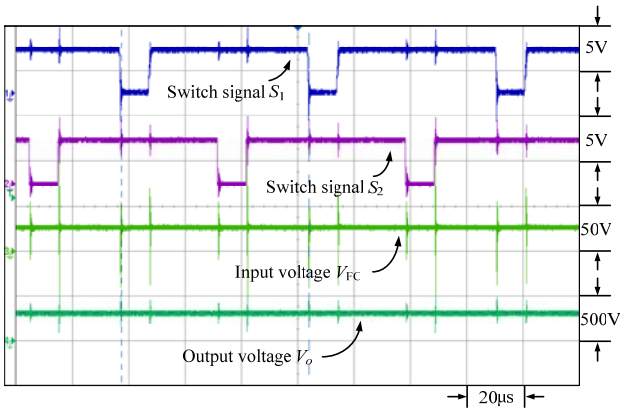

Fig. 16 The switch signal and input/output voltage waveforms under output power 200 W

Fig. 17 and Fig. 18 are the waveforms of switch signal, inductance current i_{L1} and i_{L2} under respective output power 43 W and 200 W. From the figures it is observed that with the gradual increase of loads, the inductance currents i_{L1} and i_{L2} are also on the increase to enable it to work in continuous current mode under higher output power.

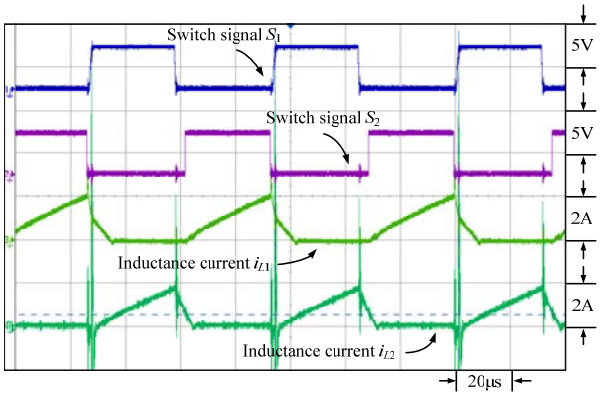

Fig. 17 The switch signal, i_{L1} and i_{L2} inductance current waveform under output power 43W

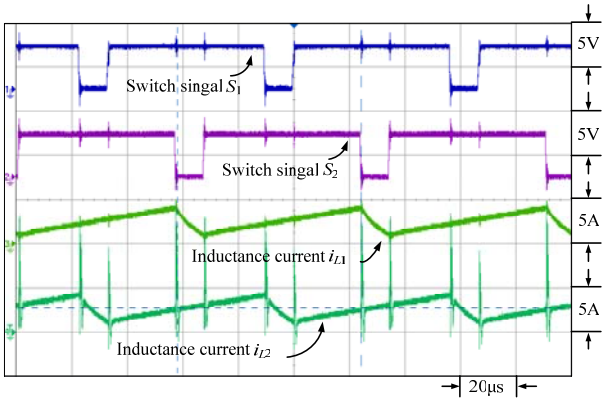

Fig. 18 The switch signal, i_{L1} and i_{L2} inductance current waveform under output power 200W

Fig. 19 and Fig. 20 are the respective output voltage ripple waveforms of single set voltage-doubler boost converter and the presented dual interleaved voltage-doubler of high voltage ratio converter. From Fig. 19 and Fig. 20 it is observed that through comparison we find there is improvement in output voltage ripple waveform. In Fig. 19 the peak to peak voltage of the single set voltage-doubler boost converter is about 15.8 V, while that of the presented dual interleaved voltage-doubler of high voltage ratio converter in Fig. 20 is about 9.5 V. Their respective voltage ripple ratios are 5.27% and 3.17%.

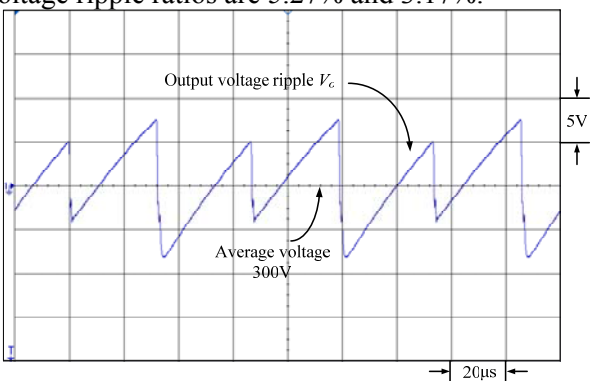

Fig. 19 The output voltage ripple waveform of single voltage-doubler boost converter under output power 43 W

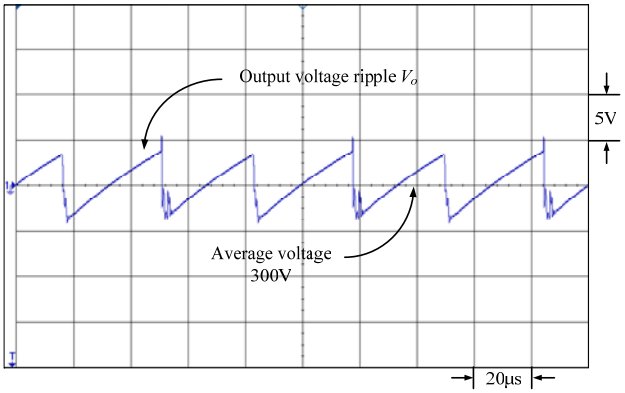

Fig. 20 The output voltage ripple waveform of the presented dual interleaved voltage-doubler of high voltage ratio converter under output power 43 W

Fig. 21 and Fig. 22 are the respective output voltage ripple waveforms of single set voltage-doubler boost converter and the presented dual interleaved voltage-doubler of high voltage ratio converter. From Fig. 21 and Fig. 22 it is observed that through comparison we find there is improvement in output voltage ripple waveform. In Fig. 21 the peak to peak voltage of the single set voltage-doubler boost converter is about 36 V, while that of the presented dual interleaved voltage-doubler of high voltage ratio converter in Fig. 22 is about 26.25 V. Their respective voltage ripple ratios are 12% and 8.75%. Thus it is proved that the dual interleaved voltage-doubler of high voltage ratio converter can improve the flaw of higher voltage ripple ratio of the original single set voltage-doubler boost converter.

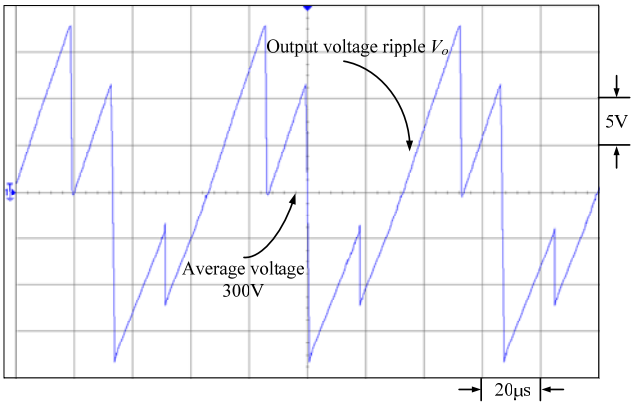

Fig. 21 The output voltage ripple waveform of single voltage-doubler boost converter under output power 200 W

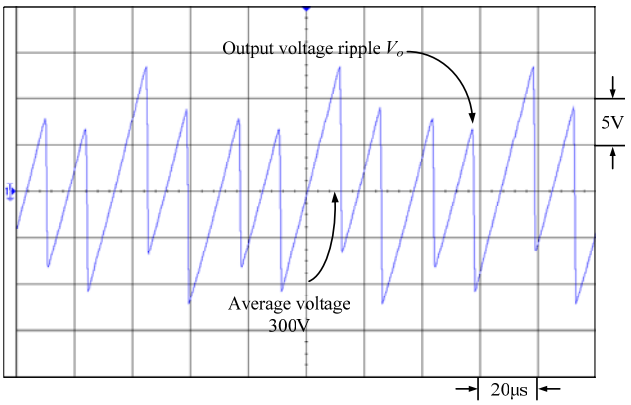

Fig. 22 The output voltage ripple waveform of the presented dual interleaved voltage-doubler of high voltage ratio converter under output power 200 W

6 Conclusion

This paper sets forth an ameliorated dual interleaved voltage-doubler of high voltage ratio converter to improve the problem of output ripple voltage of single set voltage-doubler boost converter. With two parallelly connected voltage-doubler boost converters to interleave the output voltage ripple, we further lower the output voltage ripple. Not only does it maintain the advantages of voltage doubler boost converter, but also, owing to the interleaved single set converter with two separate current routes and the two sets of switches of the double voltage-booster once again in parallel connection leading to four separate current routes, it is thus possible to further lower the current stress of the switch and inductance. Through test and experiment, this paper proves and confirms the feasibility of the presented dual interleaved converter.

7 Acknowledgement

This work was supported by the National Science Council, Taiwan, R.O.C., under the Grant of #NSC99-2623-E-167-001-ET.

References

[1] J. C. Amphlett, R. F. Mann, B. A. Peppiey, P. R. Roberge, and A. Rodrigues, A Model Predicting Transient Response of Proton Exchange Membrane Fuel Cells, *Journal of Power Source*, Vol. 61, No. 1-2, 1996, pp.183-188.

[2] R. F. Mann, J. C. Amphlett, M. A. I. Hooper, H. M. Jensen, B. A. Peppley and P. R. Roberge, Development and Application of a Generalized Steady-State Electrochemical Model for a PEM Fuel Cell, *Journal of Power Source*, Vol. 86, 2000, pp. 173-180.

[3] J. M. Correa, F. A. Farret, and L. N. Canha, An Analysis of the Dynamic Performance of Proton Exchange Membrane Fuel Cells using an Electrochemical Model, in *Proc*. *IEEE IECO'01 Conference*, 2001, pp. 141-146.

[4] D. M. Ali, A Simplified Dynamic Simulation Model (Prototype) for a Stand-Alone Polymer Electrolyte Membrane (PEM) Fuel Cell Stack, in *Proc*. *IEEE MEPCON'08 Conference*, 2008, pp. 480-485.

[5] R. J. Wai, C. Y. Lin, and C. C. Chu, High Step-up DC-DC Converter for Fuel Cell Generation System, in *Proc*. *IEEE IECO'04 Conference*, 2004, pp. 57-62.

[6] R. J. Wai and R. Y. Duan, High Step-Up Converter with Coupled-Inductor, *IEEE Transactions on Power Electronics*, Vol. 20, No. 5, 2005, pp. 1025-1035.

[7] R. J. Wai, L. W. Liu, and R. Y. Duan, High-Efficiency Voltage-Clamped DC–DC Converter with Reduced Reverse-Recovery Current and Switch-Voltage Stress, *IEEE Transactions on Industrial Electronics*, Vol. 53, No. 1, 2006, pp. 272-280.

[8] P. Thounthong, S. Rael, and B. Davat, Control Strategy of Fuel Cell and Supercapacitors Association for a Distributed Generation System, *IEEE Transactions on Industrial Electronics*, Vol. 54, No. 6, 2007, pp. 3225-3233.

[9] P. Thounthong, S. Rael, and B. Davat, Analysis of Supercapacitor as Second Source Based on Fuel Cell Power Generation, *IEEE Transactions on Energy Conversion*, Vol. 24, No. 1, 2009, pp. 247-255.

[10] S. K. Changchien, T. J. Liang, and L. S. Yang, Novel High Step-Up DC–DC Converter for Fuel Cell Energy Conversion System, *IEEE Transactions on Industrial Electronics*, Vol. 57, No. 6, 2010, pp. 2007-2017.

[11] P. Thounthong, S. Pierfederici, J.-P. Martin, M. Hinaje, and B. Davat, Modeling and Control of Fuel Cell/Supercapacitor Hybrid Source Based on Differential Flatness Control, *IEEE Transactions on Vehicular Technology*, Vol. 59, No. 6, 2010, pp. 2700-2710.

[12] A. Shahin, M. Hinaje, J.-P. Martin, S. Pierfederici, S. Rael, and B. Davat, High Voltage Ratio DC–DC Converter for Fuel-Cell Applications, *IEEE Transactions on Industrial Electronics*, Vol. 57, No. 12, 2010, pp. 3944-3955.

[13] C. T. Pan and C. M. Lai, A High-Efficiency High Step-Up Converter with Low Switch Voltage Stress for Fuel-Cell System Applications, *IEEE Transactions on Industrial Electronics*, Vol. 57, No. 6, 2010, pp. 1998-2006.

[14] Data sheet of a 1.2 kW Ballard NEXA™ Power Module, *Ballard Power Systems Inc.*, 2004 Ballard Power Systems Corp. AN2001-04.

[15] L. P. Lima, F. A. Farret, D. B. Ramos, F. Z. Ferrigolo, H. W. Stangarlin, J. G. Trapp, and A. B. Serdotte, PSIM Mathematical Tools to Simulate Pem Fuel Cells Including the Power Converter, in *Proceeding of IEEE IECO'09 Conference*, 2009, pp. 2784-2789.

[16] J. Jia, Y. Wang, Q. Li, Y. T. Cham, and M. Han, Modeling and Dynamic Characteristic Simulation of a Proton Exchange Membrane Fuel Cell, *IEEE Transactions on Energy Conversion*, Vol. 24, No. 1, 2009, pp. 283-291.

[17] Y. T. Jang and M. M. Jovanovic, Interleaved Boost Converter with Intrinsic Voltage-Doubler Characteristic for Universal-Line PFC Front End, *IEEE Transactions on Power Electronics*, Vol. 22, No. 4, 2007, pp. 1394-1401.

[18] C. T. Pan, C. M. Lai, M. C. Cheng, and L. T. Hsu, A Low Switch Voltage Stress Interleaved Boost Converter for Power Factor Correction, in *Proceeding of IEEE PEDS'09 Conference*, 2009, pp. 49-54.